Appl Phys A (2012) 107:891–897
DOI 10.1007/s00339-012-6815-8

Applied Physics A
Materials Science & Processing

Unipolar resistive switching in Au/Cr/$Mg_{0.84}Zn_{0.16}O_{2-\delta}$/$p^+$-Si

Jing Qi · Jingjian Ren · Mario Olmedo · Ning Zhan · Jianlin Liu

Received: 23 September 2011 / Accepted: 6 February 2012 / Published online: 29 February 2012

Abstract Unipolar resistive switching memory cells were fabricated using a $Mg_{0.84}Zn_{0.16}O_{2-\delta}$ thin film, sandwiched between p^+-Si (100) substrate and Cr/Au top electrodes. Electrical measurements showed a large memory window and memory window margin of 10^7 and 10^4, respectively. Furthermore, a wide switching voltage distribution gap of 3.6 V between the switching-ON and -OFF processes was obtained for different sweeping cycles. Gas bubbles at four different stages were observed on the top electrodes after electrical stimulus, indicating that conducting filaments consisting of oxygen vacancies are responsible for the resistive switching characteristics. Conductive atomic force microscopy results show that the highly conductive areas are along the edge of the gas bubble or the edge of the device. This phenomenon suggests the potential of scaling down the device area to lower than 32 nm.

1 Introduction

The electrical resistance of transition metal oxides, [1] perovskite oxides [2], and organic materials [3] can be reversibly changed between high and low resistive values under electrical stimulus, thus enabling the operation of resistive switching memory (RSM) [4]. As a promising RSM material, $Mg_xZn_{1-x}O$ has also been extensively studied [5–7]. Among these RSM materials, some have shown repeatedly unipolar switching, i.e., resistance transition under the same voltage polarity, such as NiO, [8] SiO_2, [9] and $Ba_{0.7}Sr_{0.3}TiO_3$ [10]. Unipolar RSM (URSM) is considered to be a good candidate for vertical 3-D stacking and high-density nonvolatile random access memory (RAM) [11]. Although URSM has been extensively studied, it still suffers from problems such as high power consumption, small memory window margin, and overlap of the two types of switching voltages. These problems are the main obstacles for achieving reliable URSM devices [12, 13]. The latest result on $Mg_xZn_{1-x}O$ material [7] shows that the SET voltage increases with the increase of Mg content, while the RESET voltage shows a slight change. These results indicate that alloying of ZnO and MgO might be promising for resolving these problems. However, the RESET current is still higher than 20 mA. In this paper, unipolar resistive switching characteristics of a $Mg_{0.84}Zn_{0.16}O_{2-\delta}$ thin film are investigated using Cr/Au as the top contact. The devices show a high OFF/ON resistance ratio ($>10^7$), a large memory window margin ($>10^4$), a wide voltage gap (3.6 V) between two types of switching voltage distributions, and low power consumption (100 μW). By resolving the problems of small memory window margin and voltage gap, reliable low power consumption URSM devices were achieved by using $Mg_{0.84}Zn_{0.16}O_{2-\delta}$ as the active layer. The mechanism of resistive switching is also discussed.

2 Experimental details

A continuous $Mg_{0.84}Zn_{0.16}O_{2-\delta}$ thin film (30 nm) was deposited on a pre-cleaned p^+-Si (100) substrate at 550°C using a few atomic layers of MgO as buffer in a radio frequency (RF) plasma-assisted molecular beam epitaxy (MBE) system. The pre-clean procedure consisted of a

J. Qi · J. Ren · M. Olmedo · N. Zhan · J. Liu (✉)
Department of Electrical Engineering, Quantum Structures Laboratory, University of California, Riverside, CA 92521, USA
e-mail: jianlin@ee.ucr.edu

J. Qi
Department of Physics, School of Physical Science and Technology, Lanzhou University, Lanzhou 730000, China

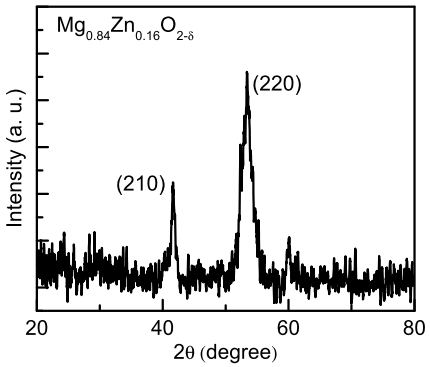

Fig. 1 GIAXRD result for $Mg_{0.84}Zn_{0.16}O_{2-\delta}$ thin film deposited on p^+-Si (100)

conventional RCA cleaning process [14] followed by annealing at 900°C for 10 minutes in an MBE chamber to remove the native oxide layer. High-purity Mg (6N) and Zn (6N) sources were evaporated from conventional low-temperature effusion cells. Atomic oxygen was provided by an RF plasma source. Cr(50 nm)/Au(50 nm) square-shaped metal patterns of 200 μm × 200 μm, which act as top electrodes, were deposited on the $Mg_{0.84}Zn_{0.16}O_{2-\delta}$ film by electron beam evaporation after photolithography, followed by a standard lift-off process. Al was evaporated onto p^+-Si (100) by an electron beam evaporator as back contact. Glancing incidence angle X-ray diffraction (GIAXRD) was utilized to check the structure of the $Mg_{0.84}Zn_{0.16}O_{2-\delta}$ film. X-ray photoelectron spectroscopy (XPS) was employed to determine the chemical composition of the thin film, yielding an Mg mole fraction of 0.84 ($Mg_{0.84}Zn_{0.16}O_{2-\delta}$), which was further confirmed by energy-dispersive X-ray spectroscopy (EDX). The electrical characteristics of the Au/Cr/$Mg_{0.84}Zn_{0.16}O_{2-\delta}$/$p^+$-Si/Al structure were measured by an Agilent 4155C semiconductor analyzer. Scanning electron microscopy (SEM) was utilized to observe surface morphology changes of the top electrodes after electrical characterization. The electrode delaminating process was performed as follows. First, Au was etched away using standard gold etchant. Second, a 200 nm Cr blanket with three layers was evaporated on the top of the devices at rates of 0.5, 1.0, and 3.0 Å/S from bottom to top, respectively. Third, both the blanket and the top Cr electrodes were removed by an adhesive tape. A Veeco Dimension Icon atomic force microscopy (AFM) instrument with conductive (C)-AFM capabilities was used for the C-AFM measurements.

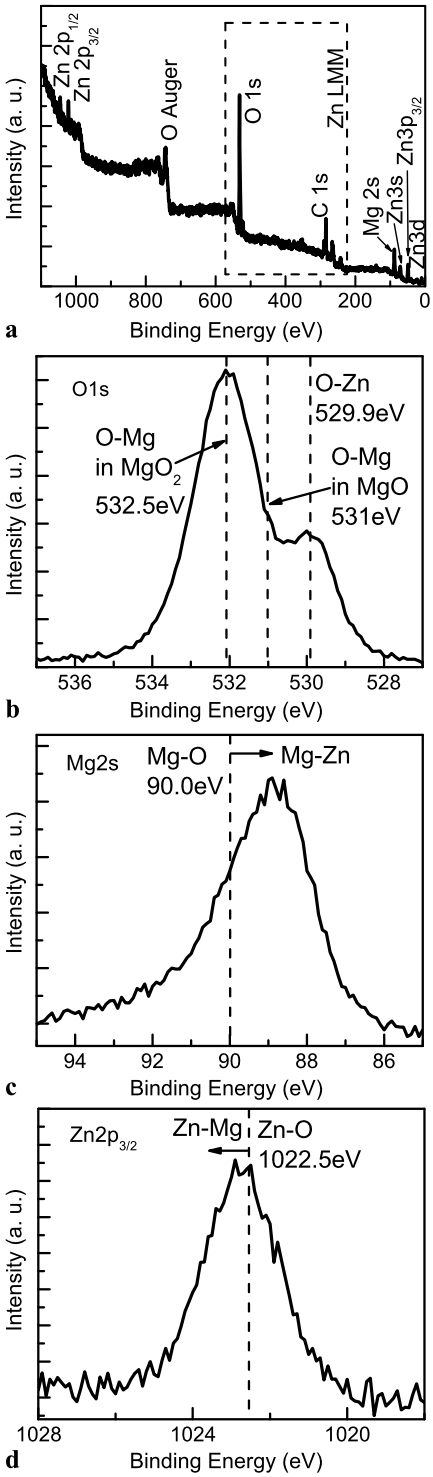

Fig. 2 (**a**) XPS survey spectrum and high-resolution scan of (**b**) O 1s, (**c**) Mg 2s, and (**d**) Zn $2p_{3/2}$ spectra for $Mg_{0.84}Zn_{0.16}O_{2-\delta}$ thin film

3 Results and discussion

Figure 1 is the GIAXRD pattern of the $Mg_{0.84}Zn_{0.16}O_{2-\delta}$ thin film. Two peaks centered at $2\theta = 53.46°$ and 41.64° can be observed, which correspond to (220) and (210) of the cubic $Mg_{0.84}Zn_{0.16}O_{2-\delta}$ thin film. The deviation of about 0.05° from the peaks of MgO_2 (JCPDS card no. 75-1585) is caused by the incorporation of Zn into the lattice of MgO_2.

XPS analysis was used to identify elements and obtain the element ratio of Zn and Mg in the film. Figure 2 shows

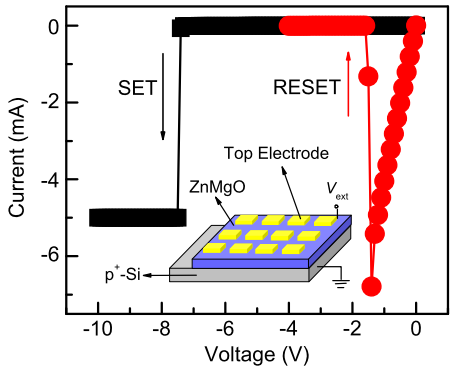

Fig. 3 Typical I–V curves of unipolar resistive switching behavior in sweep mode for RSM consisting of $Mg_{0.84}Zn_{0.16}O_{2-\delta}$ thin film (30 nm) sandwiched between a p^+-Si substrate and Cr(50 nm)/Au(50 nm) top electrodes of 200 × 200 μm^2 (*inset*)

the XPS survey spectrum and high-resolution scan of the O 1s, Mg 2s, and Zn $2p_{3/2}$ spectra of the film, in which the binding energies were calibrated using the carbon (C 1s) peak (285.0 eV) as a reference. [15] According to the XPS survey spectrum result shown in Fig. 2(a), the ratio of Mg, Zn, and O can be calculated using the method reported by Yang et al. [16] to be 0.84:0.16:1.64, meaning that the level of oxygen vacancy (δ) is 0.36 and the film composition is $Mg_{0.84}Zn_{0.16}O_{2-\delta}$. The formation of $Mg_{0.84}Zn_{0.16}O_{2-\delta}$ is further evidenced by the triple-peak structure of the O 1s emission in the high-resolution scan of the O 1s spectrum as shown in Fig. 2(b). The main peak located at 532.5 eV binding energy (the HBE peak) is accompanied by two shoulders at approximately 1.5 eV and 2.6 eV lower binding energies, respectively. The HBE peak at 532.5 eV corresponds to a species chemically similar to MgO_2. The small shoulder at 531.0 eV (1.5 eV lower binding energy) is from a structure similar to MgO, which indicates the high level of oxygen vacancy in the MgO_2 lattice. The O 1s emission of a shoulder next to the main peak as a clear evidence for the existence of nonstoichiometric MgO_2 species was also reported by other researchers [17]. The second broader shoulder at 529.9 eV is the O–Zn peak. The peak in Mg 2s (Fig. 2(c)) is no longer at 90.0 eV (Mg–O in MgO lattice), which is caused by the added Mg–O in the MgO_2 lattice and the Mg–Zn binding energy. The added Mg–Zn binding energy has also caused the high-energy shift of the peak in Zn $2p_{3/2}$ (Fig. 2(d)) from 1022.5 eV (Zn–O).

Figure 3 shows a typical current–voltage (I–V) curve of the RSMs consisting of $Mg_{0.84}Zn_{0.16}O_{2-\delta}$ thin film sandwiched by p^+-Si substrate and Cr(50 nm)/Au(50 nm) top electrodes of 200 μm × 200 μm (the device structure is shown as an inset in Fig. 3). In this device structure, the p^+-Si substrate acts as the bottom contact; its behavior is similar to that of metal because of the high doping. It is evident that these devices show typical unipolar resistive switching characteristics. The $Mg_{0.84}Zn_{0.16}O_{2-\delta}$

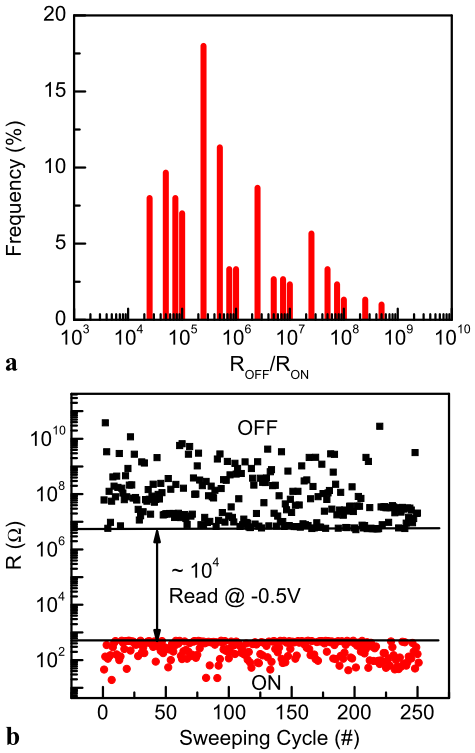

Fig. 4 (**a**) Distribution of R_{OFF}/R_{ON} for 10 measured devices. 250 cycles were measured for each device. (**b**) Switching characteristics for OFF- and ON-states measured at −0.5 V

RSMs were highly insulating in their pristine states. During the initial sweep, as the applied external voltage (V_{ext}) (0 → −10 V) in DC sweeping mode increased to approximately −7.5 V, the current increased suddenly, which switched the RSMs to the low resistance state or ON-state. This is hereby defined as the SET process, and the voltage as the SET voltage (V_{SET}) correspondingly. A current compliance of 5 mA was applied during the SET process. (If no suitable current compliance were utilized, the sudden increase of current would cause a complete dielectric breakdown, resulting in permanent damage.) Afterwards, as V_{ext} (0 → −4 V) increased from 0 to around −1.4 V, the RSMs were switched from ON to a high resistance state or OFF-state. This process was defined as RESET with a corresponding RESET voltage (V_{RESET}). Note that an electroforming process was not necessary due to the high level of oxygen vacancy.

Ten devices were measured for 250 cycles each to determine the memory window of the device, which is defined as

$$w = (R_{OFF} - R_{ON})/R_{ON} \sim R_{OFF}/R_{ON}, \quad (1)$$

where R_{OFF}, R_{ON} are the resistances of the OFF- and ON-states, respectively. The statistical results are shown in Fig. 4(a). The memory window distributes mainly between

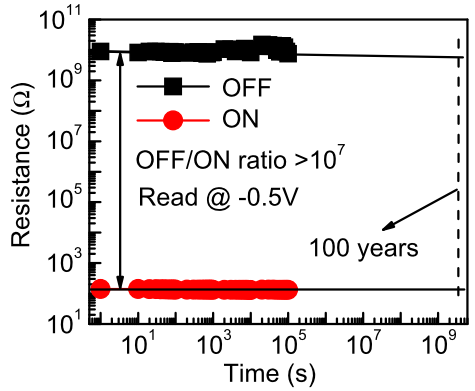

Fig. 5 Retention characteristics of the Au/Cr/MgZnO/p^+-Si RSM devices. Both OFF and ON exhibit little variation with a resistance ratio of more than 10^7 after 1×10^5 s

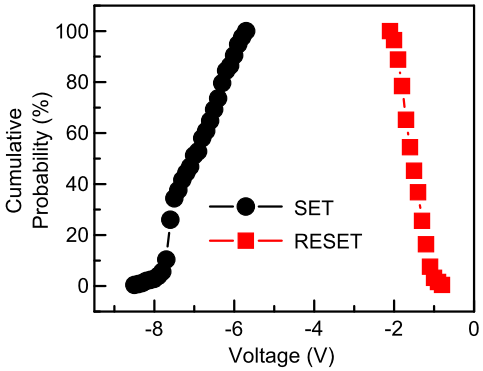

Fig. 6 Typical V_{SET} and V_{RESET} distributions of different cycles for one $Mg_{0.84}Zn_{0.16}O_{2-\delta}$ RSM device

10^5 and 10^6. The average memory window is as high as 1×10^7, which can be defined as

$$\overline{w} = \frac{\sum_{i=1}^{m}(\sum_{j=1}^{n} w_{ij})}{m \times n}, \tag{2}$$

where m is the number of devices, n is the number of the measured cycle, and w_{ij} is the memory window of the jth cycle for the ith device.

As an example, Fig. 4(b) shows the resistance values versus switching cycles for one of the ten measured devices, in which the resistance values were obtained at −0.5 V. The values of R_{OFF} and R_{ON} will fluctuate somewhat. However, the memory window margin, defined by the two resistance states as

$$w_m = \left(R_{OFF}^{min} - R_{ON}^{max}\right)/R_{ON}^{max} \sim R_{OFF}^{min}/R_{ON}^{max}, \tag{3}$$

is larger than 10^4. In formula (3), R_{OFF}^{min} and R_{ON}^{max} are the minimum resistance of the OFF-state and the maximum resistance of the ON-state in the 250 measured cycles, respectively. No RESET failure was observed for all the measurements (Fig. 4(b)). Furthermore, after 250 cycles of measurement, all devices could still be successfully SET and RESET, meaning that the endurance of the memory cells is larger than 250 cycles, which is very good [18] because the DC voltage sweeping used to operate the devices here can easily wear out memory devices [19].

The typical retention performance of Au/Cr/$Mg_{0.84}Zn_{0.16}O_{2-\delta}$/$p^+$-Si RSMs is shown in Fig. 5, in which the ON- and OFF-state resistance was measured at −0.5 V in sampling mode after the SET and RESET process, respectively. Both ON- and OFF-state with a large resistance ratio of over 10^7 exhibited little degradation after 1×10^5 s. As the data trends are extrapolated to 100 years, the two states can still be clearly distinguished without significant change in the OFF/ON resistance ratio, indicating that the retention time of this device is expected to be longer than 100 years.

For practical application of URSMs, the wide distributions in V_{SET} and V_{RESET} are considered to be a major obstacle [12, 13]. The wide distributions can lead to overlap of V_{SET} and V_{RESET}, causing failure of the RESET process and permanent damage to the devices when V_{ext} of the RESET process is larger than V_{SET}. In order to determine the distributions of V_{SET} and V_{RESET} of the devices, V_{SET} and V_{RESET} were surveyed for the above measured devices. The representative results are shown in Fig. 6. V_{RESET} and V_{SET} distribute in the ranges of −0.8 to −2.1 V and −5.7 to −8.5 V, respectively for this memory cell. The gap between the two ranges is as wide as 3.6 V because of the larger V_{SET}, which is caused by the high resistivity of $Mg_{0.84}Zn_{0.16}O_{2-\delta}$. This gap is large enough to avoid RESET failure and device damaging problems.

A reduction in RESET power is crucial for future high-density URSMs. In order to further investigate the potential for lowering the RESET power, the relationship between the RESET current (I_{RESET}) and SET current compliance (I_{CSET}) was studied. Figure 7(a) shows typical I–V characteristics for the sweeping with a SET current compliance of 500 μA and 50 μA. The statistical distribution of the RESET current value at different SET current compliances is shown in Fig. 7(b), in which 10 devices were measured for 100 cycles each at three different SET current compliances. The RESET current decreased two orders correspondingly when I_{CSET} was decreased two orders. Combining the statistical results of RESET voltage, the average RESET power can be as low as 100 μW.

To clarify the conduction and switching mechanisms of the $Mg_{0.84}Zn_{0.16}O_{2-\delta}$ RSM devices, the I–V characteristics in Fig. 3 have been redrawn in different scales for both ON and OFF, as shown in Fig. 8, in which linear fittings for the two states are also shown. The I–V curve of the ON-state exhibits a linearly ohmic behavior with a slope of 1.00 in double logarithmic scale (Fig. 8(a)), which could correspond to the formation of conducting filaments in the $Mg_{0.84}Zn_{0.16}O_{2-\delta}$ film during the SET process [20]. For

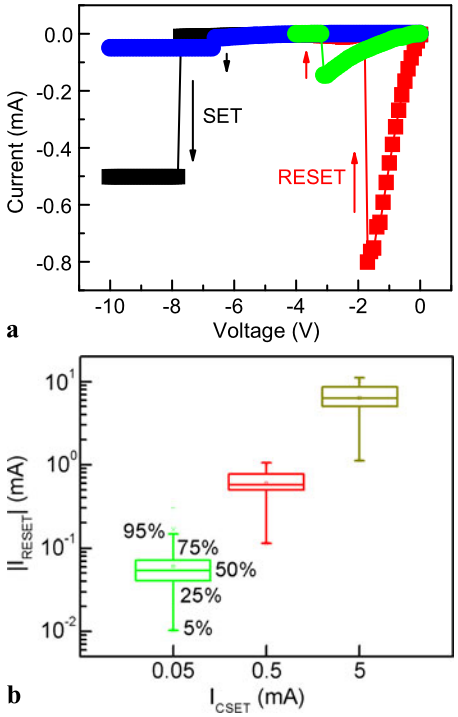

Fig. 7 (**a**) Typical I–V curve with SET current compliance of 50 μA and 500 μA. (**b**) Statistical plot of RESET current over SET current compliance (I_{CSET})

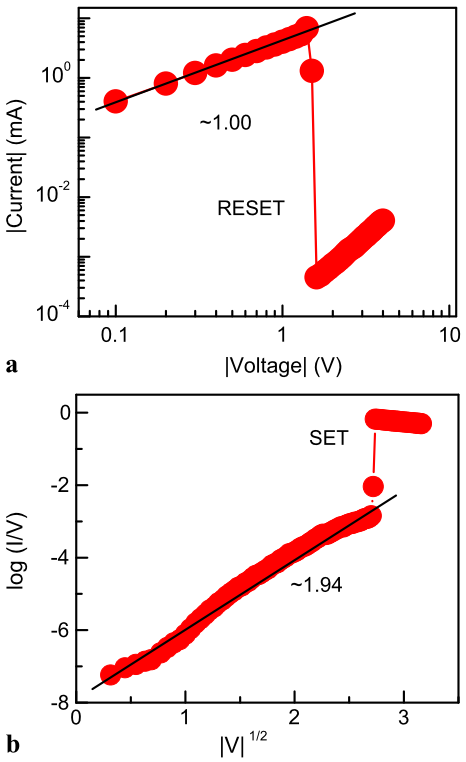

Fig. 8 Linear fittings of I–V relationship for (**a**) ON and (**b**) OFF

OFF, as shown in Fig. 8(b), the I–V characteristics can be explained by the Poole–Frenkel (PF) emission theory [21]:

$$\log(I/V) \propto \left(\sqrt{\frac{q^3}{\pi\varepsilon_r\varepsilon_0}}/rkT\right)V^{1/2} \tag{4}$$

where $q = 1.602 \times 10^{-19}$ C is the electron charge, ε_r is the dynamic dielectric constant, $\varepsilon_0 = 8.85 \times 10^{-12}$ F/m is the permittivity of free space, $k = 8.62 \times 10^{-5}$ eV/K is Boltzmann's constant, $T = 300$ K is the temperature, and r is a coefficient ranging between 1 and 2. For $r = 1$, the conduction is called the normal PF effect. For $r = 2$, the conduction is called the modified PF emission, when the insulator contains a non-negligible trap. Using $r = 2$ and the slope of $\log I/V \propto V^{1/2}$, the value of ε_r can be obtained, which is 3.6.

Furthermore, according to the conducting filament model [22, 23], during a filament formation and rupture process, the formation of a filament (SET) should be more random than the destruction of an existing filament (RESET), since the formation process is determined by the competition among different filamentary paths. Therefore, one might expect larger variations in V_{SET} than in V_{RESET}, which was validated by many other reports [24, 25]. As seen from Fig. 6, the V_{SET} distribution is indeed wider than that of V_{RESET}, which is another evidence for the conducting filament switching mechanism in this case.

The surface morphology of the top electrodes for some devices was changed after the electrical measurement. Figure 9 shows typical SEM images of the surface morphology changes. It is evident that gas-bubble and blown-off regions appear on the top electrodes. Similar gas bubble formation was previously reported in resistive RAM cells based on TiO_2 materials [20, 26]. These were caused by evolution of excess oxygen gas under the electrodes during the SET process:

$$O_O \rightarrow V_O^{\bullet\bullet} + 2e^- + \frac{1}{2}O_2, \tag{5}$$

where $V_O^{\bullet\bullet}$ denotes an oxygen vacancy having a double positive charge with respect to the regular $Mg_{0.84}Zn_{0.16}O_{2-\delta}$ lattice and O_O represents an oxygen ion on a regular site [4]. Four stages of gas bubbles were observed in one SEM image (Fig. 9(b)): (1) started, (2) formed, (3) close to blown off, and (4) blown off. A zoomed-in image of a perfectly formed bubble is also shown in the inset of Fig. 9(b). In this structure Cr acts as an oxygen reservoir due to its high oxygen affinity [27]. thus the majority of the device surface showed little or no change. The gas-bubble and blown-off regions correspond to the locations where the strongest filaments consisting of oxygen vacancies have been developed for the device [20]. The reservoirs were insufficient to contain excessive oxygen during the measurement in these regions. As a reservoir, Cr is partially oxidized to CrO_x at

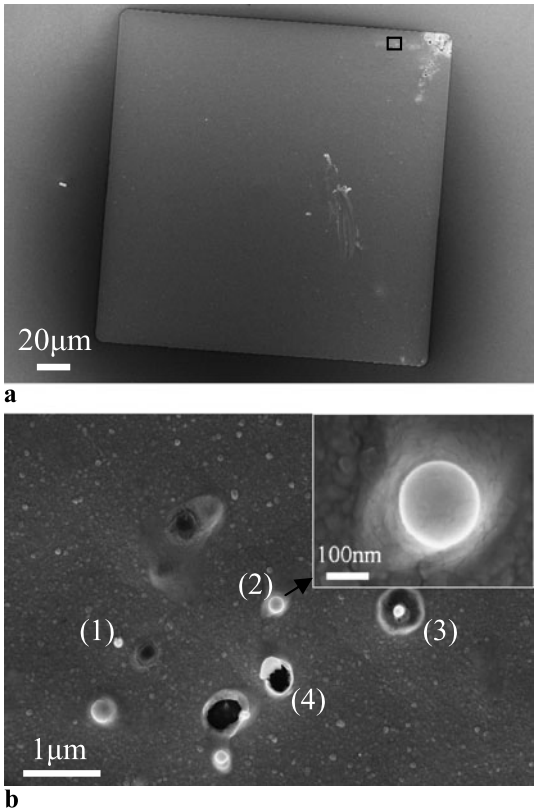

Fig. 9 SEM images for top electrodes after electrical measurement. (**a**) Whole electrode area. (**b**) Magnified area of the rectangular area in (**a**), which contains all four stages: started, formed, close to blown off, and blown off. *Inset* is a further zoomed-in image of a perfect gas bubble

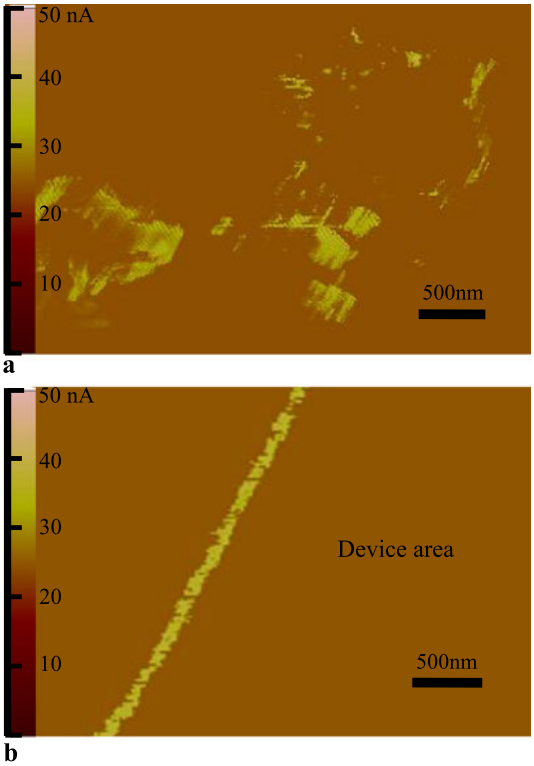

Fig. 10 C-AFM images obtained after delaminating top contacts for devices (**a**) with surface morphology change, (**b**) without surface morphology change

the Cr/$Mg_{0.84}Zn_{0.16}O_{2-\delta}$ interface, triggering the reduction process of ZnO and providing sufficient oxygen ions to neutralize the oxygen vacancies for the RESET process and stabilizing the switching property [28].

C-AFM images were taken after the top contacts were delaminated for the ON-state devices, as shown in Fig. 10. For those devices with surface change, the high conducting areas are along the edge of the blown-up area or bubble, as shown in Fig. 10(a). Similar results are also reported in TiO_2 memristive devices [29]. For those devices without surface change, the highly conductive areas are along the edge of the device (Fig. 10(b)). These results mean that the active device part is along the device edge instead of in the device center. In other words, no matter how small the device is, as long as there is a device edge, the device can be an active URSM cell. In this case, a URSM using $Mg_{0.84}Zn_{0.16}O_{2-\delta}$ as the active layer can definitely be scaled down to less than 32 nm. These results also imply that filament oxidation plays a key role in the rupture of filaments during the RESET process, in which oxygen atoms have been supplied by oxygen stored in the gas bubble or the air. The energy needed for oxidation of filaments is applied by Joule heating, resulting from localized high current distribution along the filament paths [30]. From these results, we can also conclude that many filaments rather than a single filament were formed and ruptured during the device switching process.

4 Conclusions

RSM devices fabricated with a $Mg_{0.84}Zn_{0.16}O_{2-\delta}$ thin film sandwiched between p^+-Si substrate and Cr/Au top electrodes show unipolar resistive switching characteristics with a large memory window ($>10^7$) and memory window margin ($>10^4$). The voltage gap between the V_{SET} and V_{RESET} distributions is as wide as 3.6 V, which is wide enough to avoid RESET failure and device damage for fabricating reliable URSM cells. The results of I–V characteristics, V_{SET} and V_{RESET} distribution properties, and SEM images of the top electrodes after electrical measurement prove that the formation and rupture of conducting filaments consisting of oxygen vacancies are responsible for the resistive switching behavior. Current distribution characteristics in the C-AFM images show that a URSM based on $Mg_{0.84}Zn_{0.16}O_{2-\delta}$ thin film has good potential for scaling down to lower than 32 nm.

Acknowledgements The authors acknowledge the financial support of the Focus Center Research Program on FENA and the National Natural Science Foundation of China (No. 50902065).

References

1. X. Wu, P. Zhou, J. Li, L.Y. Chen, H.B. Lv, Y.Y. Lin, T.A. Tang, Appl. Phys. Lett. **90**, 183507 (2007)
2. R. Muenstermann, T. Menke, R. Dittmann, R. Waser, Adv. Mater. **22**, 4819 (2010)
3. L.P. Ma, J. Liu, Y. Yang, Appl. Phys. Lett. **80**, 2997 (2002)
4. R. Waser, M. Aono, Nat. Mater. **6**, 833 (2007)
5. X. Chen, G. Wu, P. Jiang, W. Liu, D. Bao, Appl. Phys. Lett. **94**, 033501 (2009)
6. L. Shi, D. Shang, J. Sun, B. Shen, Appl. Phys. Express **2**, 101602 (2009)
7. X. Cao, X. Li, X. Gao, X. Liu, C. Yang, L. Chen, J. Phys. D, Appl. Phys. **44**, 015302 (2011)
8. S. Ahn, M. Lee, Y. Park, B.S. Kang, C.B. Lee, K.H. Kim, S. Seo, D. Suh, D. Kim, J. Hur, W. Xianyu, G. Stefanovich, H. Yin, I. Yoo, J. Lee, J. Park, I. Baek, B.H. Park, Adv. Mater. **20**, 924 (2008)
9. J. Yao, L. Zhong, Z. Zhang, T. He, Z. Jin, P.J. Wheeler, D. Natelson, J.M. Tour, Small **5**, 2910 (2009)
10. W. Shen, R. Dittmann, R. Waser, J. Appl. Phys. **107**, 094506 (2010)
11. M.-J. Lee, Y. Park, D.-S. Suh, E.-H. Lee, S. Seo, D.-C. Kim, R. Jung, B.S. Kang, S.-E. Ahn, C.B. Lee, D.H. Seo, Y.-K. Cha, I.-K. Yoo, J.-S. Kim, B.H. Park, Adv. Mater. **19**, 3919 (2007)
12. S.C. Chae, J.S. Lee, S. Kim, S.B. Lee, S.H. Chang, C. Liu, B. Kahng, H. Shin, D. Kim, C.U. Jung, S. Seo, M. Lee, T.W. Noh, Adv. Mater. **20**, 1154 (2008)
13. D.C. Kim, M.J. Lee, S.E. Ahn, S. Seo, J.C. Park, I.K. Yoo, I.G. Baek, H.J. Kim, E.K. Yim, J.E. Lee, S.O. Park, H.S. Kim, U. Chung, J.T. Moon, B.I. Byu, Appl. Phys. Lett. **88**, 232106 (2006)
14. W. Kern, D.A. Poutinen, RCA Rev. **31**, 187–205 (1970)
15. X.D. Peng, M.A. Barteau, Surf. Sci. **224**, 327 (1989)
16. Z. Yang, Z. Zuo, H.M. Zhou, W.P. Beyermann, J.L. Liu, J. Cryst. Growth **314**, 97 (2011)
17. C. Tegenkamp, H. Pfnur, W. Ernst, U. Malaske, J. Wollschlager, D. Peterka, K.M. Schroder, V. Zielasek, M. Henzler, J. Phys., Condens. Matter **11**, 9943–9954 (1999)
18. X. Liu, K.P. Biju, E.M. Bourim, S. Park, W. Lee, D. Lee, K. Seo, H. Hwang, Electrochem. Solid-State Lett. **14**, H9 (2011)
19. U. Russo, D. Jelmini, C. Cagli, A.L. Lacaita, S. Spiga, C. Wiemer, M. Perego, M. Fanciulli, I.E.D.M. Tech. Dig. **2007**, 775 (2007)
20. D.H. Kwon, K.M. Kim, J.H. Jang, J.M. Jeon, M.H. Lee, G.H. Kim, X.S. Li, G.S. Park, B. Lee, S. Han, M. Kim, C.S. Hwang, Nat. Nanotechnol. **5**, 148 (2010)
21. J.R. Yeargan, H.L. Taylor, J. Appl. Phys. **39**, 5600 (1968)
22. Y.C. Yang, F. Pan, Q. Liu, M. Liu, F. Zeng, Nano Lett. **9**, 1636 (2009)
23. K. Szot, W. Speier, R. Carius, U. Zastrow, W. Beyer, Phys. Rev. Lett. **88**, 075508 (2002)
24. Z. Wang, P.B. Griffin, J. McVittie, S. Wong, P.C. McIntyre, Y. Nishi, IEEE Electron Device Lett. **28**, 14 (2007)
25. B.J. Choi, D.S. Jeong, S.K. Kim, C. Rohde, S. Choi, J.H. Oh, H.J. Kim, C.S. Hwang, K. Szot, R. Waser, B. Reichenberg, S. Tiedke, J. Appl. Phys. **98**, 033715 (2005)
26. J.J. Yang, F. Miao, M.D. Pickett, D.A. Ohlberg, D.R. Stewart, C.N. Lau, R.S. Williams, Nanotechnology **20**, 215201 (2009)
27. E. Gordo, G.Z. Chen, D.J. Fray, Electrochim. Acta **49**, 2195 (2004)
28. W. Chang, H. Huang, W. Wang, C. Hou, Y. Chueh, J. He, J. Electrochem. Soc. **159**, G29–G32 (2012)
29. R. Münstermann, J.J. Yang, J.P. Strachan, G. Medeiros-Ribeiro, R. Dittmann, R. Waser, Phys. Status Solidi **4**, 16 (2010)
30. D.W. Kim, R. Jung, B.H. Park, X.S. Li, C. Park, S. Shin, D.C. Kim, C.W. Lee, S. Seo, Jpn. J. Appl. Phys. **47**, 1635 (2008)